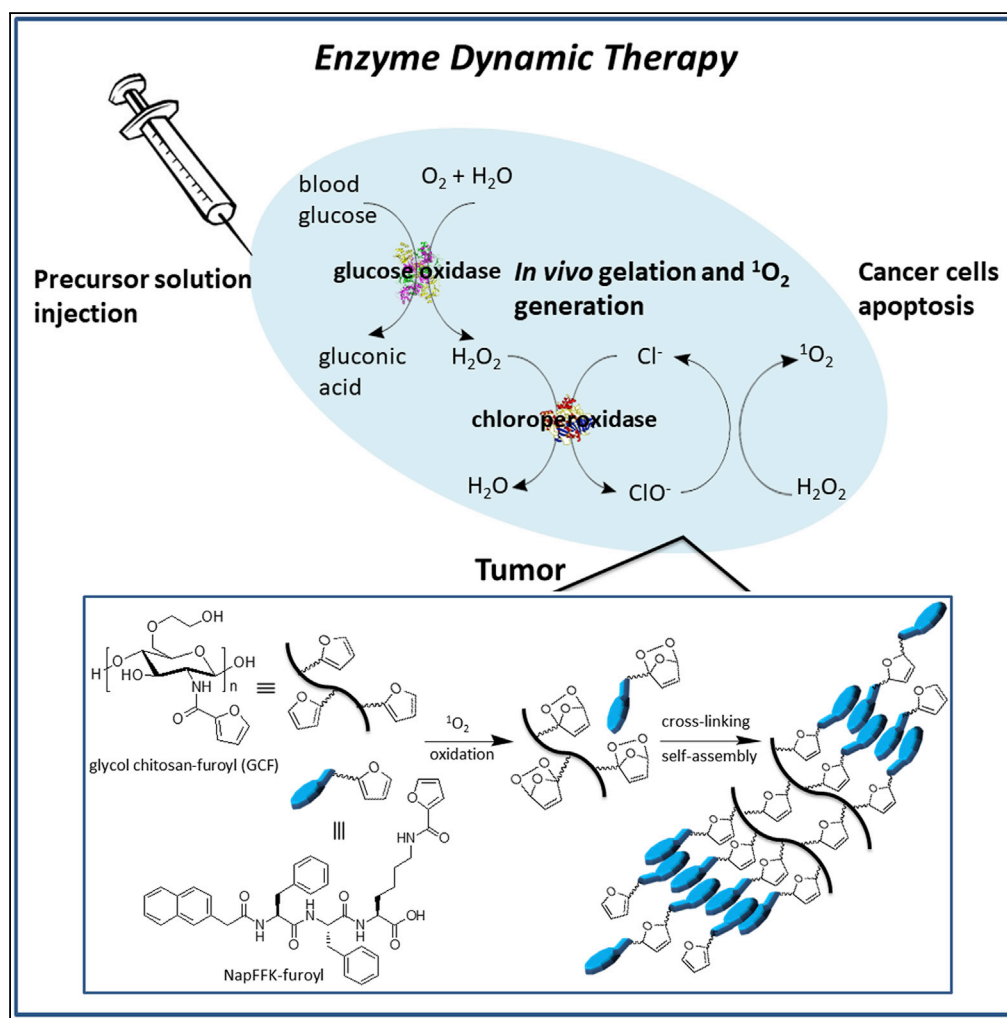


Article

Injectable Peptide Hydrogel Enables Integrated Tandem Enzymes' Superactivity for Cancer Therapy



Qingcong Wei,
Shan Jiang,
Rongrong Zhu, Xia
Wang, Shilong
Wang, Qigang
Wang

wsl@tongji.edu.cn (S.W.)
wangqg66@tongji.edu.cn
(Q.W.)

HIGHLIGHTS

Injectable peptide-based hydrogel was formed by tandem enzymatic $^1\text{O}_2$ cross-linking

Enzymes restrained in gel matrix exhibited superactivity for upregulating singlet oxygen

The hydrogel restricted enzymes within tumor rather than diffusing into normal tissues

The continuous upregulated $^1\text{O}_2$ gave the hydrogel significant antitumor efficacy

Wei et al., iScience 14, 27–35
April 26, 2019 © 2019 The
Authors.
[https://doi.org/10.1016/
j.isci.2019.03.008](https://doi.org/10.1016/j.isci.2019.03.008)

Article

Injectable Peptide Hydrogel Enables Integrated Tandem Enzymes' Superactivity for Cancer Therapy

Qingcong Wei,^{1,2} Shan Jiang,¹ Rongrong Zhu,¹ Xia Wang,¹ Shilong Wang,^{1,*} and Qigang Wang^{1,3,*}**SUMMARY**

Elevation of the levels of reactive oxygen species and other toxic radicals is an emerging strategy to treat certain cancers by modulating the redox status of cancer cells. The biocatalytic upregulation of singlet oxygen by neutrophilic leukocytes should utilize robust enzymes and design carriers with protective microenvironment. Here, we utilize GOx-CPO as integrated tandem enzymes to *in situ* generate singlet oxygen, which could be not only for oxidative cross-linking of injectable hydrogel carriers but also for continuous tumor treatment by adjustable bioconversion of blood oxygen, glucose, and chloride ion. The tandem enzymes self-restrained within peptide hydrogel exhibited superactivity for upregulating singlet oxygen relative to free enzymes, which also avoids the diffusion of enzymes from tumor. This work will not only deepen the study of enzymes in biocatalysis but also offer an enzyme therapeutic modality for treating cancers.

INTRODUCTION

Reactive oxygen species (ROS) including singlet oxygen ($^1\text{O}_2$), superoxide radicals, hydroxyl radicals, and H_2O_2 are formed as a natural by-product of the normal metabolism of oxygen, which have important roles in *cell signaling* and metabolic stability maintenance. Although the increase of ROS under environmental stimulus, called oxidative stress, is harmful to cells and organisms (Au and Madison, 2000; Balasubramanian et al., 1990; Lambrechts et al., 2005; Schrag et al., 2013; Shen et al., 1996), a high level of ROS can suppress tumor growth and resist bacterial infection. Therefore, ROS-elevating and ROS-eliminating strategies have been developed with the former being predominantly used for cancer therapy. As a successful exploration, photodynamic therapy utilizes *in situ* photosensitizers and light activation to elevate toxic ROS, especially singlet oxygen, for treating certain cancers (Celli et al., 2010). Obviously, in cells, the production of singlet oxygen rarely depends on light. In fact, the destruction of microorganism after phagocytosis by neutrophilic polymorphonuclear leukocytes relies on tandem enzymatic upregulation of ROS, which utilizes nicotinamide adenine dinucleotide phosphate oxidase to produce endogenous H_2O_2 or superoxide radical and further upregulates the singlet oxygen or hypochlorous acid level by myeloperoxidase (Klebanoff, 2005; Ying, 2008). Therefore, the bioinspired upregulation of singlet oxygen by integrating tandem enzymes could be an alternative pathway, which involves glucose oxidase (GOx) for the generation of H_2O_2 and chloroperoxidase (CPO) from *Caldariomyces fumago* to upregulate singlet oxygen.

Enzymes in organisms are spatially restricted in tiny sophisticated subcellular organelles, and tandem enzymatic reactions could have higher overall reaction efficiency, even superactivity. This could be ascribed to the fact that intermediates generated in the previous reaction could be used promptly by the next enzymatic reaction before they diffuse into cytosols. It is evident that biomimetic enzyme nanocomposites, especially enzyme cascade system, could exhibit excellent catalytic efficiency and enhanced stability via the smart scaffold design (Liu et al., 2013; Wilner et al., 2009). Inspired by this, some vehicles could be designed and used to imitate tandem enzymatic reactions. Therefore the indispensable property of the vehicle is to entrap enzymes so that it could not only effectively retain enzymes around tumor cells and improve the bioavailability but also protect enzymes to maintain their activity, thereby allowing for continuous treatment (Hah et al., 2011; Parsons et al., 2009). Injectable and self-healing supramolecular hydrogels, including peptide-based ones are a particular promising platform due to their high structural similarity with extracellular matrices (ECMs), which could offer an ideal microenvironment for enzymatic catalysis (Medina et al., 2017; Tian et al., 2014; Wang and Yang, 2012; Wang et al., 2007; Zhou et al., 2014). Previous work from our laboratory has shown that enzymes integrated in optimized gel microenvironment maintain their high catalytic activity, even superactivity (Mao et al., 2014; Su et al., 2013; Wei et al., 2016a, 2016b). To

¹School of Chemical Science and Engineering, Research Center for Translational Medicine at East Hospital, School of Life Science and Technology, Tongji University, Shanghai 200092, China

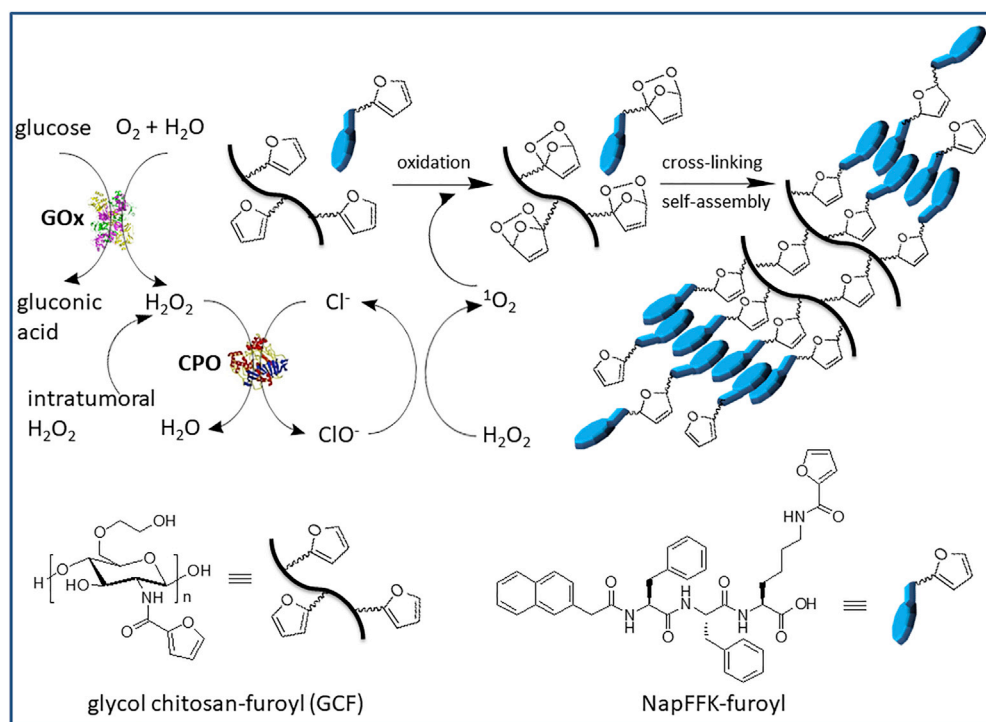
²School of Chemistry and Chemical Engineering, Henan Normal University, Xinxiang 453007, China

³Lead Contact

*Correspondence: wsl@tongji.edu.cn (S.W.), wangqg66@tongji.edu.cn (Q.W.)

<https://doi.org/10.1016/j.isci.2019.03.008>





Scheme 1. Schematic Illustration of the Hybrid Hydrogel Preparation via Dual-Enzyme (GOx and CPO)-Initiated Singlet Oxygen Cross-linking of NapFFK-furoyl (1.0 wt %) and GCF (1.0 wt %)

See also Figure S1.

enhance the antidegradable properties as biomedical vehicles (Jin et al., 2013; Puppi et al., 2010; Wang et al., 2010), peptide hydrogels could be covalently cross-linked with polysaccharide and synthetic polymers (Dai et al., 2015; Dong et al., 2017; Jeon et al., 2016; Sun et al., 2012; Yang et al., 2012). We hereby fabricated a mechanically enhanced peptide hydrogel by using *in situ* singlet oxygen cross-linking reaction (Cornwell and Smith, 2015; Schmidt and Summerer, 2013).

A novel strategy was developed by combining a GOx-mediated redox (Shenoy and Bowman, 2012; Wei et al., 2016a, 2016b; Wu et al., 2015) and a CPO-mediated redox (Kanofsky, 1984) into one cascade reaction system (Scheme 1) for controlled generation of singlet oxygen (Adam et al., 2005). Specifically, GOx oxidizes glucose to result in an elevated H₂O₂ level, which could be further used by CPO-H₂O₂-chloride system to upregulate the singlet oxygen level. Here, we prepared a furoyl-functionalized oligopeptide (NapFFK-furoyl, Figure S1A) and a furoyl derivative of glycol chitosan (GCF, Figure S1B). The peptide hydrogel with enhanced mechanical properties was then fabricated via the *in situ* singlet oxygen cross-linking catalyzed by GOx-CPO integrated tandem enzymes system, which could not only allow for rapid encapsulation of enzymes during gelation rather than diffusing into normal tissues but also enable syringe delivery of the gel into tumors. Moreover, the precursor solution containing CPO, GOx, NapFFK-furoyl, and GCF is able to form *in situ* hydrogels in tumors so that the encapsulated GOx and CPO utilize blood oxygen, glucose, and chloride to continuously generate singlet oxygen, which results in effective cancer cell apoptosis. Furthermore, the consumption of intratumoral oxygen and glucose by GOx likely starves cancer cells to death thus enhancing the anti-cancer efficacy (Fan et al., 2017; Huo et al., 2017; Li et al., 2017; Narayanan et al., 2016; Zhang et al., 2017, 2018).

RESULTS AND DISCUSSION

Preparation and Characterization of Hydrogels and Test of Singlet Oxygen Quantum Yield

We prepared the mechanically enhanced supramolecular hydrogel by simply mixing several of the following components to allow for enzyme-induced singlet oxygen cross-linking. Briefly, 5.0 mg NapFFK-furoyl was dissolved in 250 μ L alkaline solution (pH = 10), then 0.5 M HCl solution was added to adjust pH value to

7–8, and this was followed by the addition of 167 μL GCF solution (3 wt %) and the dual-enzyme-initiated system (5 mM NaCl, 15 mM glucose, 75U GOx, and 75U CPO). The total volume was adjusted to 500 μL by adding water, and the resulting solution was mixed thoroughly and kept at 37°C for 120 min to obtain hybrid hydrogels. The final concentrations of dual enzyme are both 0.15 U per 1 mg hybrid hydrogel for GOx and CPO. As shown in Scheme 1, glucose was oxidized by GOx-mediated redox reactions, and the H_2O_2 product immediately participated in the oxidation of chloride via CPO-catalyzed reactions. The generated hypochlorite subsequently reacted with H_2O_2 , and singlet oxygen was produced to oxidize the furoyl groups. The resulting endoperoxides underwent cross-linking to construct the final gel network.

Next, the morphological images obtained from scanning electron microscopy (Figures 1A and 1B) and transmission electron microscopy (Figures S2A and S2B) showed that the cross-linking process facilitated the formation of denser and more entangled irregular fibers in the hybrid gel network. These results are consistent with the frequency sweep test results (Figure 1C) that the storage modulus (G') of the hybrid hydrogel (average 534 Pa) dominated over that of the supramolecular hydrogel (average 47 Pa). This indicated that the supramolecular hydrogel's network was effectively enhanced by the polysaccharides. Moreover, the effect of enzymes on peptide self-assembling was investigated by adding enzymes into peptide pre-gel solution. Rheological results (Figure S3) showed that the gelation was not affected and the G' value (average 45 Pa) of supramolecular gel with enzymes was almost the same as that of supramolecular gel without enzymes. Therefore the effect of adding enzymes on peptide self-assembling is negligible. The gelation point was reached at approximately 180 s (Figure S4A), whereas the complete gelation process took approximately 2 h. During the gelation process, the viscosity increased gradually owing to the increasing degree of cross-linking as well as the self-assembly of peptide residues (Figure 1D). This gradual change in viscosity is a critical characteristic of enzymatic gelation system that guarantees the injectable property as well as the shape recovery after injection. Finally, the self-healing property (Figure S4B) of hybrid gels could be beneficial to its biomedical applications.

To confirm the generation of singlet oxygen from our dual-enzyme-initiated system, we used data from its electron para-magnetic resonance (EPR) spectrum as the direct evidence. 2,2,6,6-tetramethylpiperidine (TEMP) and 5,5-dimethyl-1-pyrroline-N-oxide (DMPO) were employed as the singlet oxygen trapping agent and other ROS trapping agent, respectively. As shown in Figure 1E, there were clear 1:1:1 triplet EPR signals for the free dual-enzyme system when adding TEMP, with no detectable signal upon addition of DMPO. Therefore the EPR results showed that the dual-enzyme-initiated system could effectively generate singlet oxygen without the simultaneous generation of other ROS such as superoxide and/or hydroxyl radicals. We next investigated the singlet oxygen quantum yield for free enzymes (Φ_{free}), immobilized enzymes of hybrid hydrogel (Φ_{immob}), and blank hydrogel (Φ_{blank}) in aqueous solution employing Rose Bengal (RB, $\Phi_{\text{RB}} = 0.76$) as a reference (Lin et al., 2013). Φ_{free} , Φ_{immob} , and Φ_{blank} were calculated according to the absorbance attenuation (ΔA) of 9,10-anthracenediyl-bis(methylene)dimalonic acid. The slope of a linear fitted curve corresponded to the absolute amount of singlet oxygen in which the Φ_{immob} , Φ_{free} , and Φ_{blank} were 0.71, 0.62, and 0.00 respectively (Figure 1F). The activity of the immobilized enzymes was slightly higher (1.14-fold) than that of the free enzymes, which might have resulted from the overall increased reaction efficiency promoted by the cascade reaction. It is possible that GOx and CPO might encapsulate themselves in close proximity during the gelation process. This would have allowed the product of H_2O_2 in GOx-mediated redox to be immediately utilized by CPO to generate hypochlorite and further singlet oxygen. However, GOx and CPO were separated in the free enzyme system, which resulted in a lower local concentration of generated H_2O_2 around CPO due to the partial diffusion of H_2O_2 into the bulk solution (Liu et al., 2013; Wilner et al., 2009). These results demonstrate that the dual enzyme successfully maintained their activity within the gel matrix. Moreover, the time-dependent enzymatic activity was evaluated by the same singlet oxygen quantum yield assay. Cubic pieces of 100 μL hybrid hydrogel were incubated at 37°C and tested the singlet oxygen generation at different time nodes. As shown in Figure S5, the singlet oxygen generation rate decreased gradually and reached ca. 28% after 48-h incubation. These results indicated that the dual enzyme would lose activity gradually, which would be a major parameter for the *in vivo* anti-tumor experiments.

Biocompatibility of Hydrogels and *In Vitro* Generation of Singlet Oxygen

Furthermore, we sought to determine the *in vitro* biocompatibility of both the gel matrix ingredients and the cell inactivation ability of the hybrid hydrogel via CCK8 assays. The glioblastoma cell line (U87 cells) was chosen as the model. Hydrogels were cut into fine fragments as standby. First, cells were cultured with blank hydrogel (without enzymes). No significant cytotoxic effects were observed (Figures 2A and S6) indicating that the gel matrix components had good biocompatibility under the treated

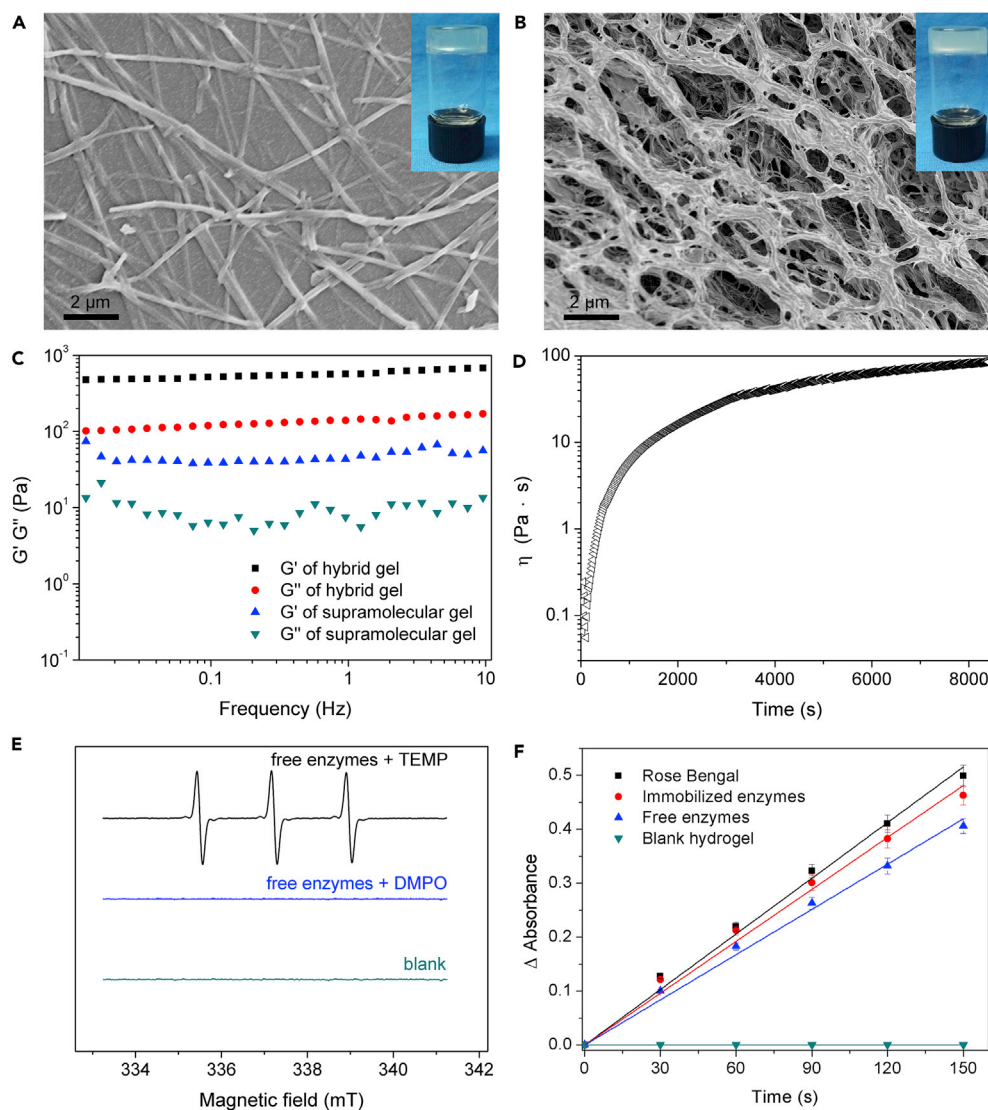


Figure 1. Morphological and Rheological Characterization, Singlet Oxygen Assay

(A and B) Scanning electron microscopic images (scale bar, 2 μm) of (A) cryo-dried supramolecular hydrogel (2 wt % NapFFK-furoyl) and (B) hybrid hydrogel (1 wt % hydrogelator and 1 wt % GC-furoyl). The inner images in (A) and (B) are supramolecular hydrogel and hybrid hydrogel, respectively. See also Figure S2.

(C) Frequency sweep tests of hybrid gel (1 wt % hydrogelator and 1 wt % GC-furoyl) and supramolecular gel (2 wt % NapFFK-furoyl) at a fixed strain of 0.2%. See also Figure S3.

(D) The viscosity test profile during the gelation process of hybrid gel. See also Figure S4.

(E) EPR spectra of dual enzymatic system in the presence of TEMP and DMPO.

(F) Singlet oxygen assay by the absorbance attenuation of 9,10-anthracenediyl-bis(methylene)dimalonic acid in various aqueous systems: Rose Bengal as positive control, immobilized enzymes of hybrid hydrogel, free enzymes, and blank hydrogel (without loading enzymes) as negative control. Error bars represent mean \pm SD ($n = 3$). See also Figure S5.

concentrations (1 $\mu\text{g/mL}$ to 100 $\mu\text{g/mL}$ hydrogel). Then, the cytotoxicity of hybrid hydrogel was evaluated. Results shown in Figure S6 indicated a relative higher cell viability (>100%) at low concentrations (1 $\mu\text{g/mL}$ to 5 $\mu\text{g/mL}$), whereas there was an increasing cytotoxicity with hybrid hydrogel in excess of 5 $\mu\text{g/mL}$ (Figure 2A). Therefore the elevated therapeutic singlet oxygen gave the hybrid hydrogel significant cell proliferation inhibition, with an IC_{50} of approximately 31 $\mu\text{g/mL}$ (ca. 4.65×10^{-3} U/mL for both GOx and CPO). The cytotoxicity of free enzymes by using the same amount of enzyme as hybrid hydrogel group was shown in Figure S7. The results exhibited similar cell viability as that of hybrid hydrogel,

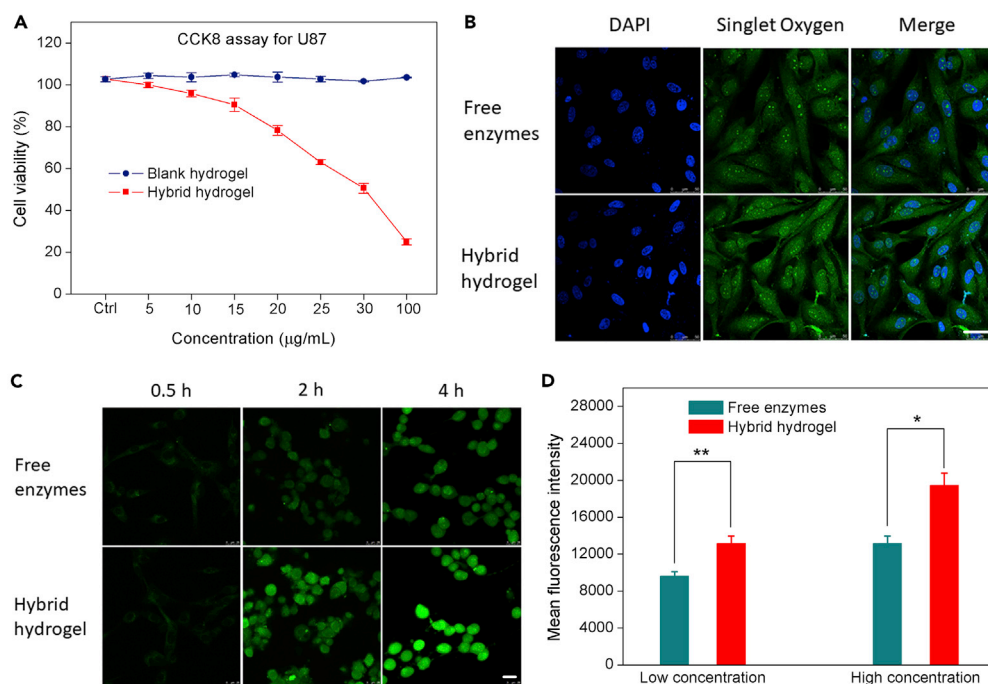


Figure 2. Cell Viability and *In Vitro* Singlet Oxygen Generation

(A) Cell viability of U87 with different concentrations of blank hydrogel and hybrid hydrogel. See also Figures S6 and S7.

(B) Oxidized SOSG confocal fluorescence images of U87 cells with free enzymes (0.3×10^{-3} U/mL for both GOx and CPO) and hybrid hydrogel (2 µg/mL) after 12-h incubation. Scale bar, 50 µm.

(C) Oxidized SOSG confocal fluorescence images of U87 cells with free enzymes (0.015 U/mL for both GOx and CPO) and hybrid hydrogel (100 µg/mL) at different time intervals. Scale bar, 50 µm.

(D) Mean fluorescence intensity in (B) and (C) at 4 h. Statistical evaluation was conducted by using analysis of variance (Student's t test).

Error bars represent mean \pm SD ($n = 3$). p value < 0.05 was considered statistically significant. ** $p < 0.01$, * $p < 0.05$.

with an IC_{50} of approximately 6.20×10^{-3} U/mL for both GOx and CPO. Overall, the accumulative damage of fatty acids, proteins, and DNA by singlet oxygen might ultimately lead to cell apoptosis, giving it an anti-cancer effect (Kriska et al., 2005; Maes et al., 2011; Nam et al., 2016). In addition, the degradation behavior of the hybrid hydrogels was evaluated by incubating gels in PBS (pH = 7.4) for 120 h. Results in Figure S8 showed that the dry weight of hybrid hydrogels decreased gradually and eventually reached a plateau after 72 h incubation. The weight loss (ca. 32%) might be due to the loss of uncross-linked peptide molecules.

To better understand free enzymes and hybrid-hydrogel-mediated singlet oxygen generation in tumor cells, free enzyme and hybrid-hydrogel-loaded U87 cells were incubated with Singlet Oxygen Sensor Green (SOSG) (Flors et al., 2006)—which could be rapidly oxidized by singlet oxygen to a green fluorescent molecule (SOSG endoperoxides, SOSG-EPs). As shown in Figure 2B, strong green fluorescence was observed by confocal laser scanning microscopy (CLSM) in each group after 12-h incubation at a low gel concentration (2 µg/mL) with a well fusiform shape of cells. Furthermore, the fluorescence intensity (Figure 2D) of hybrid-hydrogel-treated cells was slightly higher than that of free-enzyme-treated cells, indicating a high level of singlet oxygen generation, which suggested the higher anticancer efficacy of hybrid hydrogel than free enzymes. The same results could also be obtained at a higher gel concentration (100 µg/mL) as shown in Figure 2C. CLSM images (Figure 2C) revealed stronger green fluorescence (Figure 2D) in hybrid hydrogel group indicating a higher concentration of SOSG-EPs accumulated in cells incubated with hybrid hydrogel as compared with free enzymes. Furthermore, as shown in Figure 2C, fluorescence intensity gradually increased over time and cell morphology became spherical from its previous fusiform shape. Collectively, these results are consistent with the singlet oxygen quantum yield of Φ_{free} and Φ_{immob} (Figure 1F). Moreover, *in vitro* experimental results indicate that an encapsulated dual enzyme in the hybrid hydrogel could effectively upregulate the level of singlet oxygen, resulting in effective

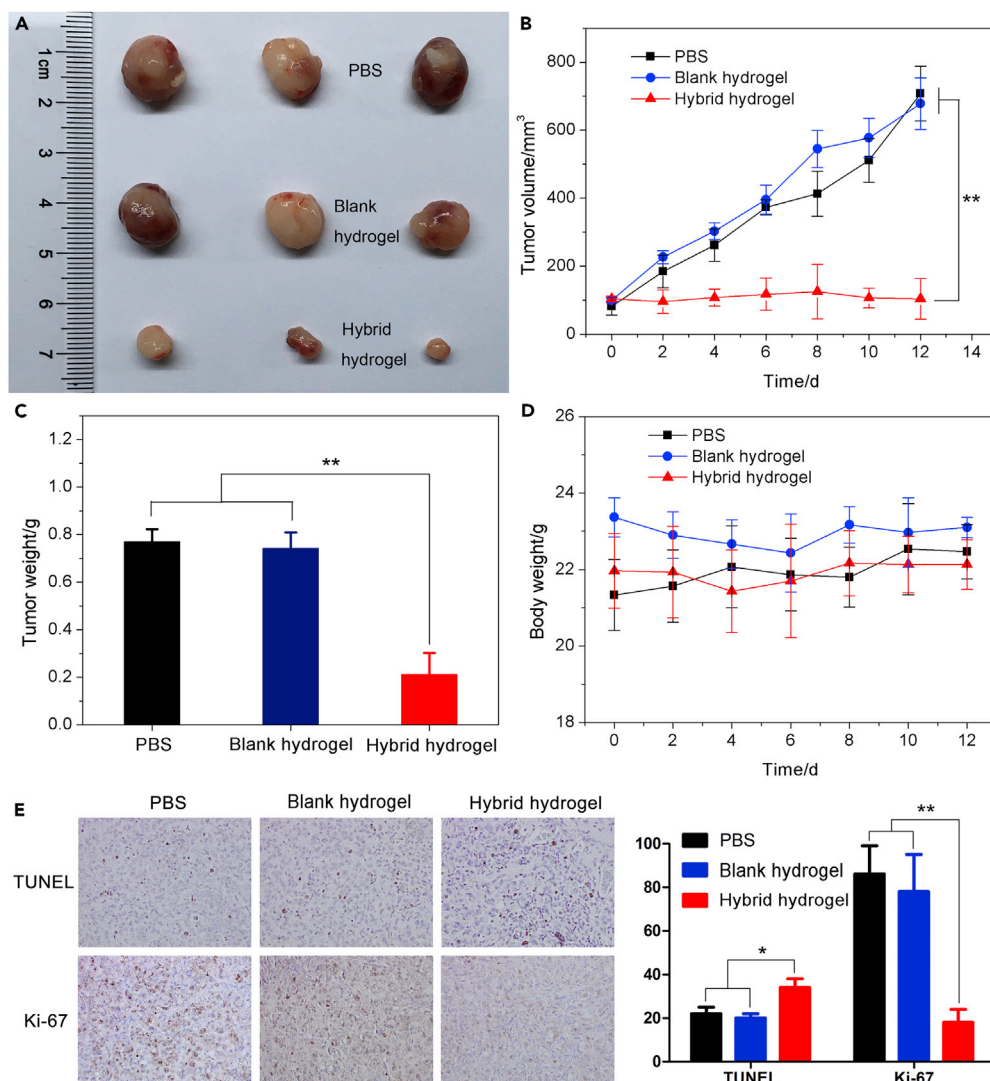


Figure 3. In Vivo Anti-tumor Experiments

(A) Photographs of the collected U87 tumor tissues after intra-tumoral injection with physiological saline, blank hydrogel, and hybrid hydrogel at day 12.

(B) Tumor volume changes of the three groups over the course of the treatments.

(C) Tumor weight changes of the three groups over the course of the treatments.

(D) Body weights of mice in different groups after treatment.

(E) TUNEL and Ki-67 immunostaining of xenografts. The positive expressions turn to brown color. Statistical evaluation was conducted by using analysis of variance (Student's t test).

Error bars represent mean \pm SD (n = 3). p value < 0.05 was considered statistically significant. **p < 0.01, *p < 0.05. See also Figures S8 and S9.

inhibition of the proliferation of tumor cells. Therefore, these results laid a solid foundation for the following *in vivo* antitumor experiments.

In Vivo Antitumor Property

At last, tumor-bearing mice were weighed and randomly divided into different treatment groups. When the tumor volume reached 100 mm³, subjects were given a single intratumoral dose (10 μ L) of PBS, blank hydrogel (oligopeptide + chitosan), or hybrid hydrogel (hydrogel 454.5 mg/kg, GOx 68.2 U/kg, and CPO 68.2 U/kg) every other day. On day 12, mice were euthanized and the tumors were collected, washed, weighed three times with saline, and fixed in 10% neutral-buffered formalin. As shown in Figure 3A, the

hybrid hydrogel significantly inhibited tumor growth compared with the other two groups. There was a slight increase in tumor volume in the hybrid hydrogel group (104.06 mm³). However, a rapid growth in tumor volume for the physiological saline (707.88 mm³) and blank hydrogel (678.42 mm³) treatment groups was observed (Figure 3B). Furthermore, the tumor weight was also minimal for the hybrid hydrogel group (Figure 3C). These results demonstrated not only that the hybrid hydrogel could effectively immobilize the dual enzyme in its matrix but also that the immobilized dual enzyme could effectively generate singlet oxygen to kill tumor cells. Besides, the body weights of the mice injected with either blank hydrogel or hybrid hydrogel were like those of mice receiving PBS, indicating a negligible toxicity for mice in both these groups (Figure 3D). The further histological response of these external stimuli on major organs of the mice were evaluated by H&E staining after the treatments, and no noticeable tissue damages and side effects were found (Figure S9). Therefore integrated tandem enzymes can be used for the non-invasive cancer therapy.

In addition, the *in vivo* Ki-67 and TUNEL (terminal deoxynucleotidyl transferase dUTP nick end labeling) detection in nude mice bearing U87 xenografts treated with PBS, blank hydrogel, and hybrid hydrogel was performed by immunohistochemistry. As shown in Figure 3E, TUNEL assay was used for detection of cell apoptosis. There were only a few positive cells in mice treated with PBS and blank hydrogel. However, a significantly increased ratio of TUNEL-positive cells was observed in hybrid-hydrogel-treated group, which proved the apoptotic induction effect of hybrid hydrogel on U87 xenografts. Furthermore, hybrid hydrogel inhibited cancer cell proliferation in a much stronger manner than PBS and blank hydrogel, as evidenced by Ki-67 staining.

DISCUSSION

In summary, we have prepared an injectable, mechanically enhanced supramolecular hydrogel by using singlet oxygen oxidative cross-linking of furoyl-functionalized oligopeptide and glycol chitosan. The hydrogel could be intratumorally injected due to their shear-thinning property from supramolecular hydrogel networks and the increasing viscosity, which could effectively immobilize enzymes within tumor rather than diffusing into normal tissues. GOx and CPO are likely restricted in the ECM-like gel networks at a close distance, and H₂O₂ generated by GOx-mediated redox reaction could be used promptly by CPO-chloride catalytic system, resulting in the superactivity of immobilized dual enzyme when compared with that of the free dual enzyme. The continuous generation of upregulated singlet oxygen by integrated tandem enzyme reaction gave the hydrogel significant *in vitro* and *in vivo* antitumor efficacy. Therefore, this injectable peptide hydrogel provides a tool for localized delivery of enzymes for high-efficiency and ROS-responsive deep-seated tumor therapy.

Limitations of Study

The control of free enzymes has not been tested *in vivo* because free enzymes could cause discomfort (even death) of the mice after intratumoral injection.

METHODS

All methods can be found in the accompanying [Transparent Methods supplemental file](#).

DATA AND SOFTWARE AVAILABILITY

The authors provide detailed description of methods and original data upon request.

SUPPLEMENTAL INFORMATION

Supplemental Information can be found online at <https://doi.org/10.1016/j.isci.2019.03.008>.

ACKNOWLEDGMENTS

This work was supported by the National Natural Science Foundation of China (No. 51473123, 31570849, 51402215, 81671105), the National Key Research and Development Program (No. 2016YFA0100800), the Scientific Research Foundation for Doctors (No. qd16112) and Youth Foundation (No. 2016QK11) of Henan Normal University.

AUTHOR CONTRIBUTIONS

Conceptualization, S.W. and Q. Wang; Methodology, R.Z., X.W., S.W., and Q. Wang; Investigation, Q. Wei, S.J., S.W., and Q. Wang; Writing – Original Draft, Q. Wei and S.J.; Writing – Reviewing & Editing, S.W. and

Q. Wang; Funding Acquisition, Q. Wei, X.W., S.W., and Q. Wang. Q. Wei, and S.J. contributed equally to this work.

DECLARATION OF INTERESTS

The authors declare no competing interests.

Received: November 1, 2018

Revised: February 15, 2019

Accepted: March 8, 2019

Published: April 26, 2019

REFERENCES

- Adam, W., Kazakov, D.V., and Kazakov, V.P. (2005). Singlet-oxygen chemiluminescence in peroxide reactions. *Chem. Rev.* *105*, 3371–3387.
- Au, V., and Madison, S.A. (2000). Effects of singlet oxygen on the extracellular matrix protein collagen: oxidation of the collagen crosslink histidinohydroxylisnonorleucine and histidine. *Arch. Biochem. Biophys.* *384*, 133–142.
- Balasubramanian, D., Du, X., and Zigler, J.S., Jr. (1990). The reaction of singlet oxygen with proteins, with special reference to crystallins. *Photochem. Photobiol.* *52*, 761–768.
- Celli, J.P., Spring, B.Q., Rizvi, I., Evans, C.L., Samkoe, K.S., Verma, S., Pogue, B.W., and Hasan, T. (2010). Imaging and photodynamic therapy: mechanisms, monitoring, and optimization. *Chem. Rev.* *110*, 2795–2838.
- Cornwell, D.J., and Smith, D.K. (2015). Expanding the scope of gels - combining polymers with low-molecular-weight gelators to yield modified self-assembling smart materials with high-tech applications. *Mater. Horizons* *2*, 279–293.
- Dai, X.Y., Zhang, Y.Y., Gao, L.N., Bai, T., Wang, W., Cui, Y.L., and Liu, W.G. (2015). A mechanically strong, highly stable, thermoplastic, and self-healable supramolecular polymer hydrogel. *Adv. Mater.* *27*, 3566–3571.
- Dong, Y.X., Sigen, A., Rodrigues, M., Li, X.L., Kwon, S.H., Kosaric, N., Khong, S., Gao, Y.S., Wang, W.X., and Gurtner, G.C. (2017). Injectable and tunable gelatin hydrogels enhance stem cell retention and improve cutaneous wound healing. *Adv. Funct. Mater.* *27*, 1606619.
- Fan, W., Lu, N., Huang, P., Liu, Y., Yang, Z., Wang, S., Yu, G., Liu, Y., Hu, J., He, Q., et al. (2017). Glucose-responsive sequential generation of hydrogen peroxide and nitric oxide for synergistic cancer starving-like/gas therapy. *Angew. Chem. Int. Ed.* *56*, 1229–1233.
- Flors, C., Fryer, M.J., Waring, J., Reeder, B., Bechtold, U., Mullineaux, P.M., Nonell, S., Wilson, M.T., and Baker, N.R. (2006). Imaging the production of singlet oxygen *in vivo* using a new fluorescent sensor, Singlet Oxygen Sensor Green (R). *J. Exp. Bot.* *57*, 1725–1734.
- Hah, H.J., Kim, G., Lee, Y.E.K., Orringer, D.A., Sagher, O., Philbert, M.A., and Kopelman, R. (2011). Methylene blue-conjugated hydrogel nanoparticles and tumor-cell targeted photodynamic therapy. *Macromol. Biosci.* *11*, 90–99.
- Huo, M.F., Wang, L.Y., Chen, Y., and Shi, J.L. (2017). Tumor-selective catalytic nanomedicine by nanocatalyst delivery. *Nat. Commun.* *8*, 357.
- Jeon, I., Cui, J.X., Illeperuma, W.R.K., Aizenberg, J., and Vlassak, J.J. (2016). Extremely stretchable and fast self-healing hydrogels. *Adv. Mater.* *28*, 4678–4683.
- Jin, J., Xing, Y.Z., Xi, Y.L., Liu, X.L., Zhou, T., Ma, X.X., Yang, Z.Q., Wang, S.T., and Liu, D.S. (2013). A triggered DNA hydrogel cover to envelop and release single cells. *Adv. Mater.* *25*, 4714–4717.
- Kanofsky, J.R. (1984). Singlet oxygen production by chloroperoxidase-hydrogen peroxide-halide systems. *J. Biol. Chem.* *259*, 5596–5600.
- Klebanoff, S.J. (2005). Myeloperoxidase: friend and foe. *J. Leukoc. Biol.* *77*, 598–625.
- Kriska, T., Korytowski, W., and Girotti, A.W. (2005). Role of mitochondrial cardiolipin peroxidation in apoptotic photokilling of 5-aminolevulinic-acid-treated tumor cells. *Arch. Biochem. Biophys.* *433*, 435–446.
- Lambrechts, S.A.G., Aalders, M.C.G., and Van Marle, J. (2005). Mechanistic study of the photodynamic inactivation of *Candida albicans* by a cationic porphyrin. *Antimicrob. Agents Chemother.* *49*, 2026–2034.
- Li, S.Y., Cheng, H., Xie, B.R., Qiu, W.X., Zeng, J.Y., Li, C.X., Wan, S.S., Zhang, L., Liu, W.L., and Zhang, X.Z. (2017). Cancer cell membrane camouflaged cascade bioreactor for cancer targeted starvation and photodynamic therapy. *ACS Nano* *11*, 7006–7018.
- Lin, H.Y., Shen, Y., Chen, D.F., Lin, L.S., Wilson, B.C., Li, B.H., and Xie, S.S. (2013). Feasibility study on quantitative measurements of singlet oxygen generation using singlet oxygen sensor green. *J. Fluoresc.* *23*, 41–47.
- Liu, Y., Du, J.J., Yan, M., Lau, M.Y., Hu, J., Han, H., Yang, O.O., Liang, S., Wei, W., Wang, H., et al. (2013). Biomimetic enzyme nanocomplexes and their use as antidotes and preventive measures for alcohol intoxication. *Nat. Nanotechnol.* *8*, 187–192.
- Maes, M., Galecki, P., Chang, Y.S., and Berk, M. (2011). A review on the oxidative and nitrosative stress (O&NS) pathways in major depression and their possible contribution to the (neuro) degenerative processes in that illness. *Prog. Neuropsychopharmacol. Biol. Psychiatry* *35*, 676–692.
- Mao, Y.J., Su, T., Wu, Q., Liao, C.A., and Wang, Q.G. (2014). Dual enzymatic formation of hybrid hydrogels with supramolecular-polymeric networks. *Chem. Commun.* *50*, 14429–14432.
- Medina, S.H., Michie, M.S., Miller, S.E., Schnermann, M.J., and Schneider, J.P. (2017). Fluorous phase-directed peptide assembly affords nano-peptisomes capable of ultrasound-triggered cellular delivery. *Angew. Chem. Int. Ed.* *56*, 11404–11408.
- Nam, J.S., Kang, M.G., Kang, J., Park, S.Y., Lee, S.J.C., Kim, H.T., Seo, J.K., Kwon, O.H., Lim, M.H., Rhee, H.W., et al. (2016). Endoplasmic reticulum-localized iridium(III) complexes as efficient photodynamic therapy agents via protein modifications. *J. Am. Chem. Soc.* *138*, 10968–10977.
- Narayanan, K., Erathodiyil, N., Gopalan, B., Chong, S., Wan, A.C.A., and Ying, J.Y. (2016). Targeting warburg effect in cancers with PEGylated glucose. *Adv. Healthc. Mater.* *5*, 696–701.
- Parsons, C., McCoy, C.P., Gorman, S.P., Jones, D.S., Bell, S.E.J., Brady, C., and McGlinchey, S.M. (2009). Anti-infective photodynamic biomaterials for the prevention of intraocular lens-associated infectious endophthalmitis. *Biomaterials* *30*, 597–602.
- Puppi, D., Chiellini, F., Piras, A.M., and Chiellini, E. (2010). Polymeric materials for bone and cartilage repair. *Prog. Polym. Sci.* *35*, 403–440.
- Schmidt, M.J., and Summerer, D. (2013). Red-light-controlled protein-RNA crosslinking with a genetically encoded furan. *Angew. Chem. Int. Ed.* *52*, 4690–4693.
- Schrag, M., Mueller, C., Zabel, M., Crofton, A., Kirsch, W.M., Ghribi, O., Squitti, R., and Perry, G. (2013). Oxidative stress in blood in Alzheimer's disease and mild cognitive impairment: a meta-analysis. *Neurobiol. Dis.* *59*, 100–110.
- Shen, H.R., Spikes, J.D., Kopeckova, P., and Kopecek, J. (1996). Photodynamic crosslinking of proteins. I. Model studies using histidine- and lysine-containing N-(2-hydroxypropyl) methacrylamide copolymers. *J. Photochem. Photobiol. B* *34*, 203–210.
- Shenoy, R., and Bowman, C.N. (2012). Kinetics of interfacial radical polymerization initiated by a glucose-oxidase mediated redox system. *Biomaterials* *33*, 6909–6914.

- Su, T., Zhang, D., Tang, Z., Wu, Q., and Wang, Q.G. (2013). HRP-mediated polymerization forms tough nanocomposite hydrogels with high biocatalytic performance. *Chem. Commun. (Camb.)* 49, 8033–8035.
- Sun, J.Y., Zhao, X.H., Illeperuma, W.R.K., Chaudhuri, O., Oh, K.H., Mooney, D.J., Vlassak, J.J., and Suo, Z.G. (2012). Highly stretchable and tough hydrogels. *Nature* 489, 133–136.
- Tian, Y., Wang, H.M., Liu, Y., Mao, L.N., Chen, W.W., Zhu, Z.N., Liu, W.W., Zheng, W.F., Zhao, Y.Y., Kong, D.L., et al. (2014). A peptide-based nanofibrous hydrogel as a promising DNA nanovector for optimizing the efficacy of HIV vaccine. *Nano Lett.* 14, 1439–1445.
- Wang, H.M., and Yang, Z.M. (2012). Short-peptide-based molecular hydrogels: novel gelation strategies and applications for tissue engineering and drug delivery. *Nanoscale* 4, 5259–5267.
- Wang, L.S., Chung, J.E., Chan, P.P.Y., and Kurisawa, M. (2010). Injectable biodegradable hydrogels with tunable mechanical properties for the stimulation of neurogenesis differentiation of human mesenchymal stem cells in 3D culture. *Biomaterials* 31, 1148–1157.
- Wang, Q.G., Yang, Z.M., Zhang, X.Q., Xiao, X.D., Chang, C.K., and Xu, B. (2007). A supramolecular-hydrogel-encapsulated hemin as an artificial enzyme to mimic peroxidase. *Angew. Chem. Int. Ed.* 46, 4285–4289.
- Wei, Q.C., Xu, M.C., Liao, C.A., Wu, Q., Liu, M.Y., Zhang, Y., Wu, C.T., Cheng, L.M., and Wang, Q.G. (2016a). Printable hybrid hydrogel by dual enzymatic polymerization with superactivity. *Chem. Sci.* 7, 2748–2752.
- Wei, Q.C., Xu, W., Liu, M.Y., Wu, Q., Cheng, L.M., and Wang, Q.G. (2016b). Viscosity-controlled printing of supramolecular-polymeric hydrogels via dual-enzyme catalysis. *J. Mater. Chem. B* 4, 6302–6306.
- Wilner, O.I., Weizmann, Y., Gill, R., Lioubashevski, O., Freeman, R., and Willner, I. (2009). Enzyme cascades activated on topologically programmed DNA scaffolds. *Nat. Nanotechnol.* 4, 249–254.
- Wu, Q., Wang, X., Liao, C.A., Wei, Q.C., and Wang, Q.G. (2015). Microgel coating of magnetic nanoparticles via bienzyme-mediated free-radical polymerization for colorimetric detection of glucose. *Nanoscale* 7, 16578–16582.
- Yang, B., Zhang, Y.L., Zhang, X.Y., Tao, L., Li, S.X., and Wei, Y. (2012). Facilely prepared inexpensive and biocompatible self-healing hydrogel: a new injectable cell therapy carrier. *Polym. Chem.* 3, 3235–3238.
- Ying, W.H. (2008). NAD(+)/NADH and NADP(+)/NADPH in cellular functions and cell death: regulation and biological consequences. *Antioxid. Redox Signal.* 10, 179–206.
- Zhang, C., Ni, D., Liu, Y., Yao, H., Bu, W., and Shi, J. (2017). Magnesium silicide nanoparticles as a deoxygenation agent for cancer starvation therapy. *Nat. Nanotechnol.* 12, 378–386.
- Zhang, R., Feng, L.Z., Dong, Z.L., Wang, L., Liang, C., Chen, J.W., Ma, Q.X., Zhang, R., Chen, Q., Wang, Y.C., et al. (2018). Glucose & oxygen exhausting liposomes for combined cancer starvation and hypoxia-activated therapy. *Biomaterials* 162, 123–131.
- Zhou, J., Du, X.W., Gao, Y., Shi, J.F., and Xu, B. (2014). Aromatic-aromatic interactions enhance interfiber contacts for enzymatic formation of a spontaneously aligned supramolecular hydrogel. *J. Am. Chem. Soc.* 136, 2970–2973.

ISCI, Volume 14

Supplemental Information

**Injectable Peptide Hydrogel Enables
Integrated Tandem Enzymes' Superactivity
for Cancer Therapy**

Qingcong Wei, Shan Jiang, Rongrong Zhu, Xia Wang, Shilong Wang, and Qigang Wang

Transparent Methods:

1. Materials

Glucose oxidase (GOx) from *Aspergillus niger*, Chloroperoxidase (CPO) from *Caldariomyces fumago*, 9,10-anthracenediyl-bis(methylene)dimalonic acid (ABDA) and glycol chitosan (GC) were purchased from Sigma-Aldrich. (Benzotriazol-1-yloxy)tris(dimethylamino)phosphonium hexafluorophosphate (BOP) was purchased from Energy-Chemical Co., Ltd (Shanghai). All amino acids used in SPPS were purchased from GL Biochem (Shanghai) Ltd. Glucose, piperidine, 2-furoic acid and other reagents were purchased from Sinopharm Chemical Reagent Co., Ltd. (Shanghai). All materials were used as received.

2. Synthesis of NapFFK-furoyl and GC-furoyl

2-(Naphthalen-2-yl)acetyl-(L)-Phe-(L)-Phe-(L)-Lys-furoyl (NapFFK-furoyl) was synthesized via standard solid phase peptide synthesis (SPPS) on a 2-chlorotriyl chloride resin by successive coupling of Fmoc-protected-L-amino acids[S1, S2]. After completion of the synthesis, peptides were cleaved from the resin via treatment of TFA/DCM (10:90, v/v) for 30 min. Peptides were then precipitated in cold diethyl ether, and the crude peptides were further purified through semi-preparative reverse-HPLC on a PRC-ODS 20 mm × 25 cm column (Shimadzu, Japan). ¹H NMR (400 MHz, DMSO-d₆) δ 8.39 (t, J = 8.38, 1H), 8.30 (t, J = 8.28, 2H), 8.18 (d, J = 8.17, 1H), 7.86 (d, J = 7.85, 1H), 7.79 (s, 1H), 7.77 (s, 1H), 7.74 (d, J = 7.73, 1H), 7.58 (s, 1H), 7.43-7.49 (m, 2H), 7.15-7.24 (m, 11H), 7.06 (d, J = 7.06, 1H), 6.60 (m, 1H), 4.56-4.59 (m, 1H), 4.48-4.53 (m, 1H), 4.16-4.22 (m, 1H), 3.46-3.59 (dd, J = 3.52, 2H), 3.18-3.21 (m, 2H), 3.07-2.67 (m, 4H), 1.76-1.30 (m, 6H). ESI-TOF m/z calcd. for C₄₁H₄₂N₄O₇ M⁺ = 702.3053, obsvd. (M + Na)⁺ = 725.2947.

GC (1 eq. -NH₂) was dissolved in 30 mL DMSO and then a solution containing 2-furoic acid (1 eq.) and BOP (1 eq.) in DMSO was added dropwise. The resulting mixture was stirred at 30 °C for 24 h. After dialyzing for 3 days against distilled water (dialysis membrane cutoff 3500), the reaction mixture was lyophilized to obtain GC-furoyl (GCF) as a fluffy solid. ¹H NMR (400 MHz, D₂O) δ 7.67 (s, 1H), 7.20-7.10 (d, J = 7.15, 1H), 6.61 (s, 1H), 4.05-2.91 (m, 16H).

3. Hydrogel preparation

Supramolecular hydrogel: NapFFK-furoyl (10.0 mg) was dissolved in 400 μL NaOH solution. Then 0.5M HCl solution was added carefully until the pH reached 7-8, the volume was adjusted to 500 μL by adding water. After the mixture was mixed thoroughly on vortex, the colorless transparent solution was kept at 25 °C for 30 min and the gel (2.0 wt% of NapFFK-furoyl) was formed.

Hybrid hydrogel: NapFFK-furoyl (5.0 mg) was dissolved in 250 μL alkaline solution (pH = 10). The pH was adjusted to 7-8 by using 0.5 M HCl solution and 167 μL GCF aqueous solution (3 wt%) was added. Then dual enzyme initiated system (5 mM NaCl, 15 mM glucose, 75U GOx and 75U CPO) was added and the total volume was adjusted to 500 μL by adding water. The resulting solution was mixed thoroughly

and kept at 37 °C for 120 min to obtain the hybrid hydrogel.

Blank hydrogel: The procedure is the same as that of hybrid hydrogel except dual enzyme initiated system.

4. SEM and TEM characterization

SEM: Hydrogel samples were coated on the silicon wafer, then frozen in liquid nitrogen, and further dried 24 h in vacuum. A thin layer of gold was sputter-coated before testing with a field emission scanning electron microscopy (Hitachi S-4800) at 3 KV voltages.

TEM: The samples were coated on the carbon-coated copper grids and stained with sodium phosphotungstate (2 wt% in water). The pictures were acquired with a transmission electron microscopy (JEM-2010) at a 80 KV voltage.

5. Rheological tests

The rheological properties of hydrogels were tested using a RS6000 rheometer (Thermo Scientific, Karlsruhe, Germany) with parallel plate geometry (35 mm diameter, 0.3 mm gap) at 37 °C. The frequency-dependent sweep was taken as a function of angular frequency at fixed strain of 0.2 %. The self-healing process of the dynamic gel in response to applied shear forces was performed using continuous step strain sweep test with alternate small oscillation force ($\gamma = 0.2 \%$) and large one ($\gamma = 200 \%$).

6. Electron Paramagnetic Resonance (EPR) measurements

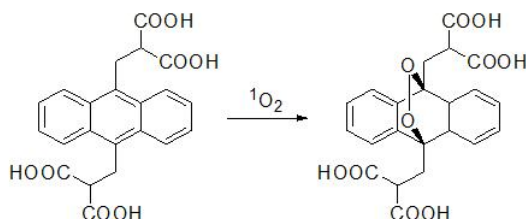
The EPR spectra were recorded on a JEOL Spectrometer (JES FA200) operating at 9.50 GHz. In a typical process, an appropriate amount of dual enzyme initiated system solution (5 mM NaCl, 15 mM glucose, 0.15U/ μ L GOx and 0.15U/ μ L CPO) was rapidly added to a standard capillary and placed into the EPR spectrometer. 2,2,6,6-tetramethylpiperidine (TEMP) and 5,5-dimethyl-1-pyrroline-N-oxide (DMPO) were used as singlet oxygen and other reactive oxygen species (ROS) trapping agents respectively. The spectra were recorded after 1 min reaction.

7. Evaluation of the singlet oxygen quantum yield

Singlet oxygen production of free enzymes and immobilized enzymes was monitored by following the loss of absorbance at 358 nm of ABDA in aqueous and the singlet oxygen quantum yield for free enzymes (Φ_{free}) and immobilized enzymes (Φ_{immob}) was calculated according to the absorbance attenuation of ABDA by employing Rose Bengal (RB, $\Phi_{\text{RB}} = 0.76$) as a reference. In a typical process, dual enzyme initiated system solution (5 mM NaCl, 15 mM glucose, 0.15U/ μ L GOx and 0.15U/ μ L CPO) 100 μ L (or cubic pieces of 100 μ L new prepared hybrid hydrogel) was added to a solution containing 20 μ M ABDA with a total volume 2 mL. The absorbance at 358 nm was recorded by a UV-Vis spectrometer (UV-2700, Shimadzu) at 30 s intervals.

In addition, the time-dependent enzymatic activity was evaluated by using the same singlet oxygen quantum yield test method. Cubic pieces of 100 μ L hybrid

hydrogel were incubated at 37 °C as standby. Three pieces of hydrogel were used at 0 h, 6 h, 12 h, 24 h, 36 h, 48 h, 72 h and 96 h respectively. The singlet oxygen quantum yield at 0 h (Φ_0) was recorded as standard. The time-dependent singlet oxygen generation rate was calculated by the following formula: Singlet Oxygen Generation Rate (%) = $\Phi_n \cdot 100 / \Phi_0$, n represents the time nodes (0, 6, 12, 24, 36, 48, 72 and 96).



8. Cell culture

A commercial glioblastoma cell line (U87 cells) was originally obtained from Type Culture Collection of the Chinese Academy of Sciences, Shanghai, China. U87 cells were cultured in DMEM medium containing 10% fetal bovine serum, 100 units/mL penicillin, and 100 mg/mL streptomycin in a humidified incubator under 5% CO₂ at 37 °C.

9. Degradation behavior of the hybrid hydrogel

To investigate the degradation behavior, 24 pieces of 0.5 mL hybrid hydrogel were divided equally into eight groups. Seven groups of hybrid hydrogel were incubated in 20 mL PBS (pH = 7.4) respectively. The weight of cryo-dried hybrid hydrogel without incubating in PBS was record as W_1 . Hybrid hydrogel was taken out from PBS one group at a time (6 h, 12 h, 24 h, 36 h, 48 h, 72 h, 96 h and 120 h), then then cryo-dried and weighted (W_2). The degradation rate was represented by the weight remained rate, calculating by the following formula: Weight Remained Rate (%) = $W_2 \cdot 100 / W_1$.

10. Cytotoxicity assay

CCK8 assay was used to assess the metabolic activity of U87 cancer cells. Hydrogels were cut into fine fragments as standby. Briefly, U87 cells were seeded into 96-well plates. After 24 h incubation, cells were treated with various concentrations of blank hydrogel, hybrid hydrogel and the same amount of enzymes as hybrid hydrogel. After incubation for 24 h in dark, the cells were incubated with a 10 μ L CCK8 for 4 h at 37 °C. The absorbance was quantified at 450 nm using the Elx 800 Universal Microplate Reader (BIO-TEK, INC).

11. *In vitro* detecting singlet oxygen burst

U87 cells were seeded in a confocal dish and incubated at 37 °C in 5% CO₂ for 24 h. Free enzymes and hybrid hydrogel (hydrogel + enzymes) were delivered into cells in DMEM culture medium for different time. Then, the cells were washed with PBS buffer to remove the nanoparticles outside the cells and fresh DMEM medium containing 10% fetal bovine serum medium was added. After fixed with 4% (v/v) formaldehyde and stained with Singlet Oxygen Sensor Green (SOSG) and

4',6-diamidino-2-phenylindole (DAPI) for 15 minutes at room temperature, the cells were examined with confocal laser scanning microscope (CLSM, Leica TCS SP5, Leica Microsystems GmbH, Germany) with 405 nm (DAPI) and 504 nm (Singlet Oxygen) excitation.

12. *In vivo* antitumor experiment

The animal experiments were conducted in accordance with the guidelines of the National Institutes of Health of China for the care and use of laboratory animals. All animal work was approved and conducted under the guidelines of Tongji University's Animal Care and Use Committee. To create the tumor-bearing mice, U87 cells were harvested by incubation with 0.05% trypsin-EDTA. Then, cells were pelleted by centrifugation and resuspended in sterile PBS. Finally, U87 cells (5×10^6 cells/site) were implanted subcutaneously into the right forelimb of four- to five-weeks-old female athymic nude mice, respectively. The tumor-bearing mice were weighed and randomly divided into different groups when the tumor volume grew to 100 mm^3 , and 10 μL PBS, oligopeptide-chitosan blank hydrogel, or hybrid hydrogel (hydrogel 454.5 mg/kg, GOx 68.2U/kg and CPO 68.2U/kg) was injected into each tumor of mice in group every other day, and meanwhile the tumor size was measured. At Day 12, the mice were euthanized, and the tumors were collected, washed, weighed with saline thrice and fixed in the 10% neutral-buffered formalin. The tumor size was examined by vernier caliper and calculated via the formula below. Tumor volume = (Tumor Length)*(Tumor Width)²/2.

We've also conducted the *in vivo* antitumor experiments of free enzymes. We found free enzymes could cause discomfort (even death) of the mice after intratumoral injection due to the reason that free enzymes easily diffuses into normal tissues, while hydrogel could encapsulate enzymes firmly in the gel matrix, effectively preventing their diffusion and maintaining activity.”

13. Immunostaining

Briefly, paraffin-embedded sections were deparaffinized, rehydrated, and microwave heated for antigen retrieval. After blocking, the rabbit polyclonal antibody Terminal deoxyribonucleotide transferase-mediated nick-end labeling (TUNEL) staining was done using the *in situ* Cell Death Detection kit (Roche Applied Science, Indianapolis, IN) following the instructions of the manufacturer. Ki-67 (SANTA CRUZ BIOTECHNOLOGY, INC) at 1:100 dilution was applied and incubated overnight at 4 °C, and the slides were applied with biotinylated secondary antibody.

14. Figures

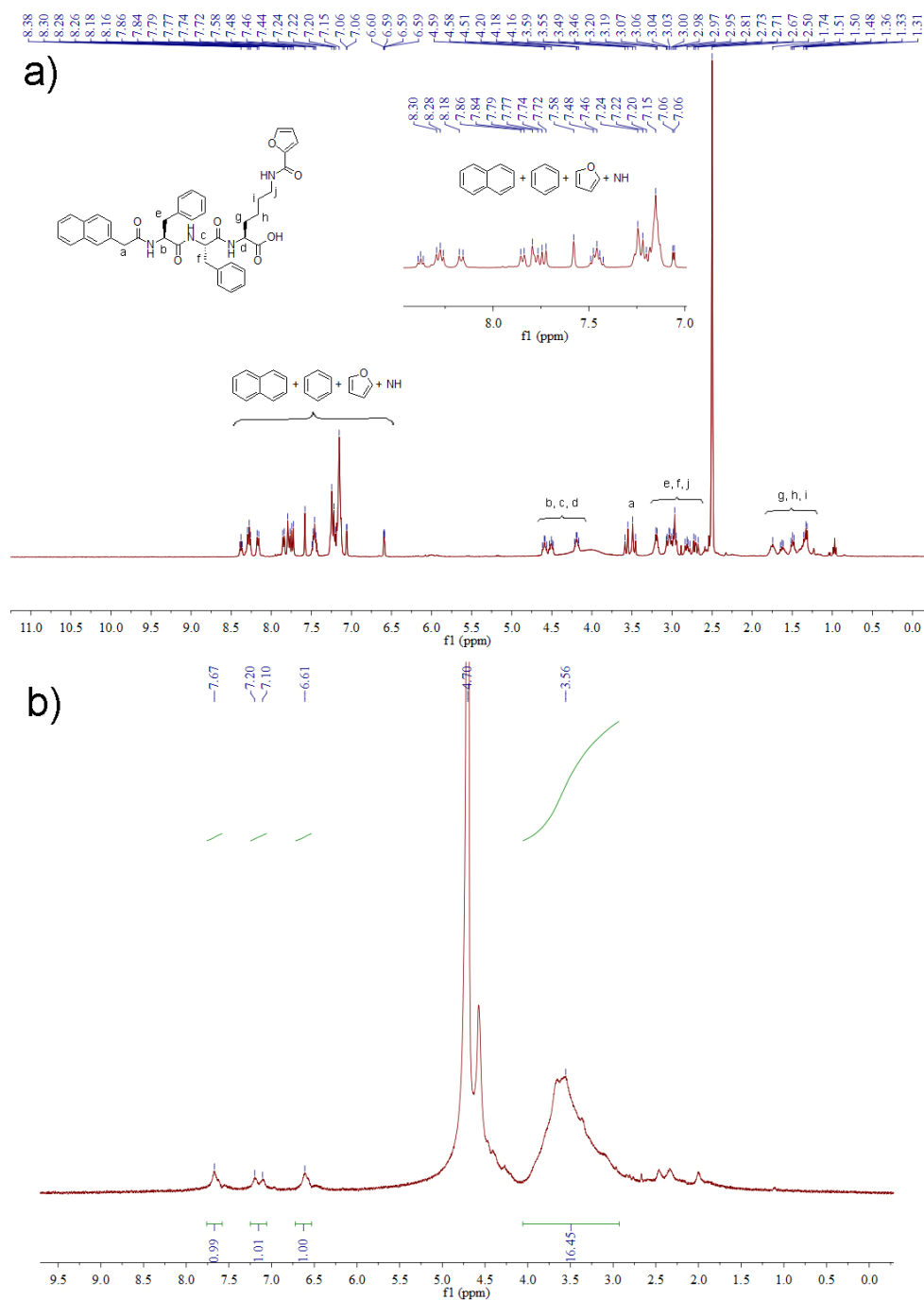


Figure S1, related to Scheme 1. ¹H NMR spectra: (a) NapFFK-furoyl in DMSO-d₆. (b) GC-furoyl in D₂O, the modification degree of furoyl ($\delta = 6.61$, 1H) relative to GC backbone ($\delta = 2.9-4.1$, 5H) is calculated according to the integration, and the result is ca. 0.3.

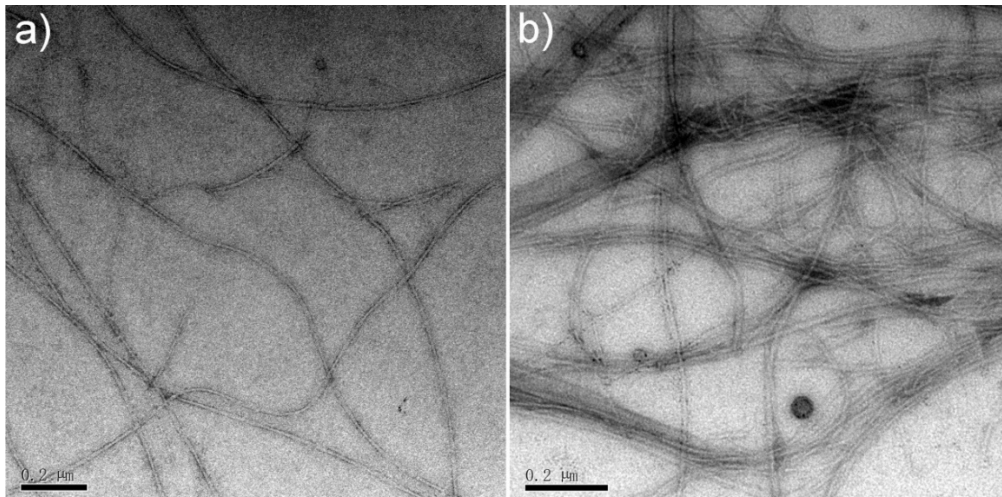


Figure S2, related to Figure 1A and 1B. TEM images (scale bar 0.2 μm) of negatively stained fibrils of supramolecular hydrogel (a) and hybrid hydrogel (b).

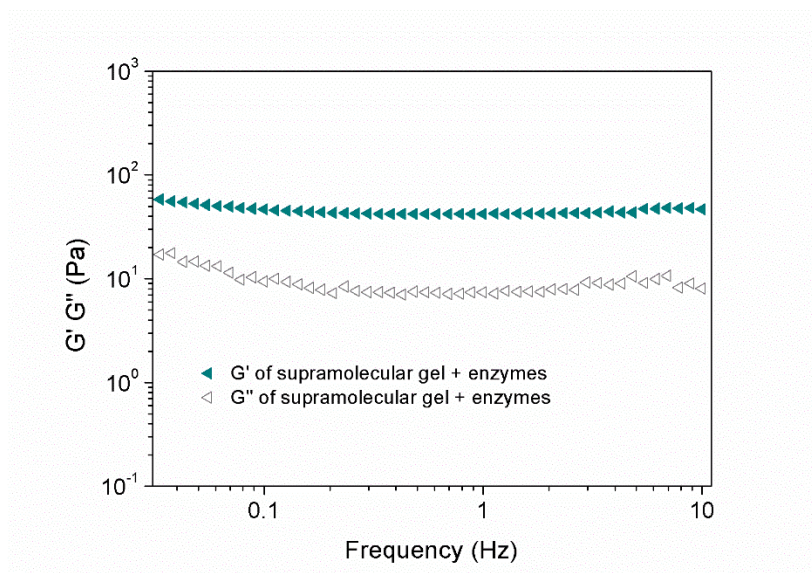


Figure S3, related to Figure 1C. Frequency sweep tests of supramolecular gel + enzymes (2 wt% NapFFK-furoyl) at a fixed strain of 0.2%.

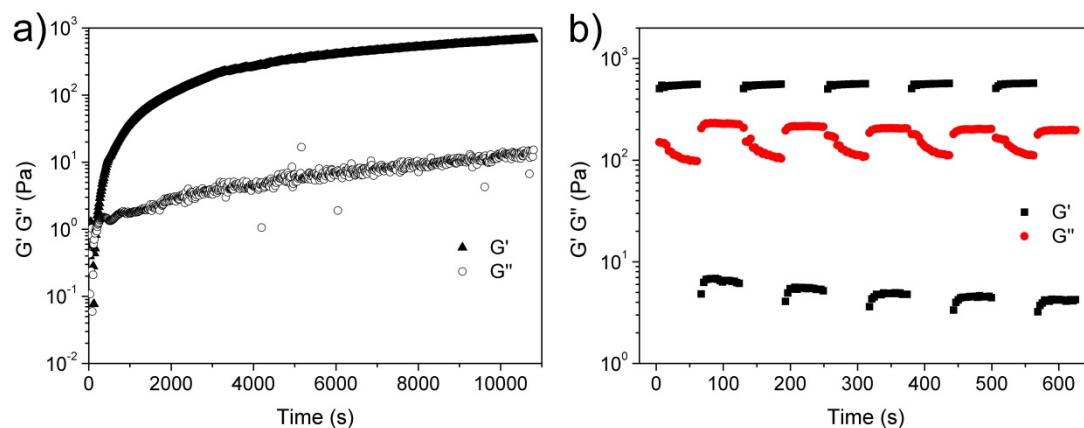


Figure S4, related to Figure 1D. (a) The time sweep test profile of hybrid gel (GOx 5U/ μ L, CPO 5U/ μ L) at a fixed strain of 0.2 %; (b) The self-healing property test with alternate small oscillation force ($\gamma = 0.2\%$) and large one ($\gamma = 200\%$).

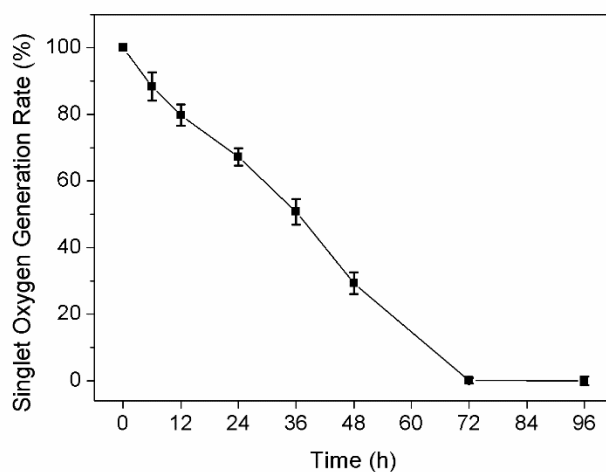


Figure S5, related to Figure 1F. The singlet oxygen generation rate profile was used to evaluate the time-dependent enzymatic activity.

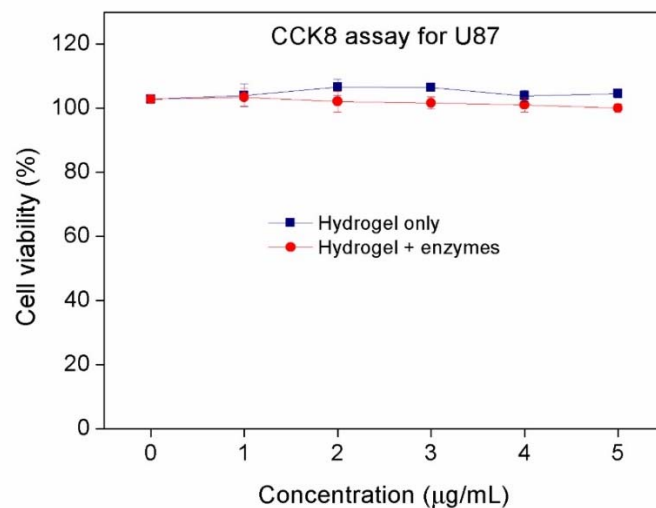


Figure S6, related to Figure 2A. Cell viability of U87 with different concentrations of hydrogel only and hybrid hydrogel (hydrogel + enzymes).

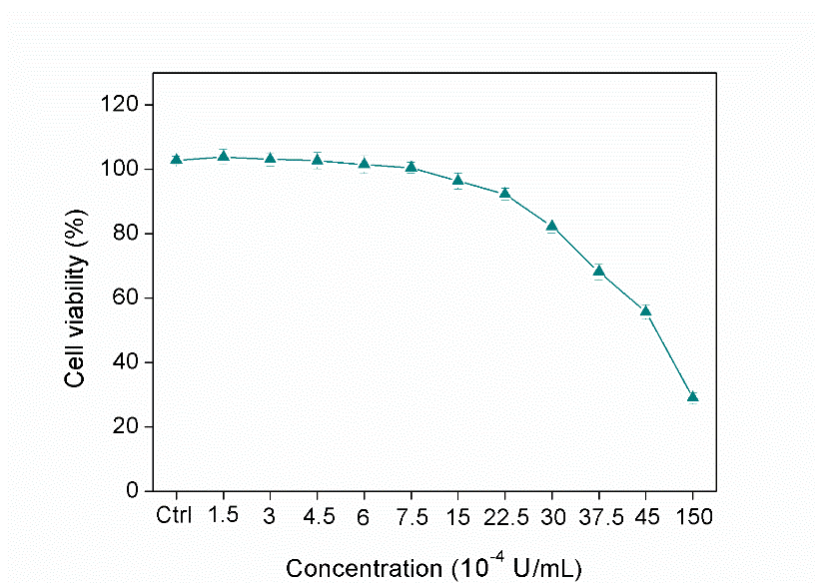


Figure S7, related to Figure 2A. Cell viability of U87 with different concentrations of free enzymes by using the same amount of enzymes as hybrid hydrogel, with an IC_{50} approximately 6.20×10^{-3} U/mL for both GOx and CPO.

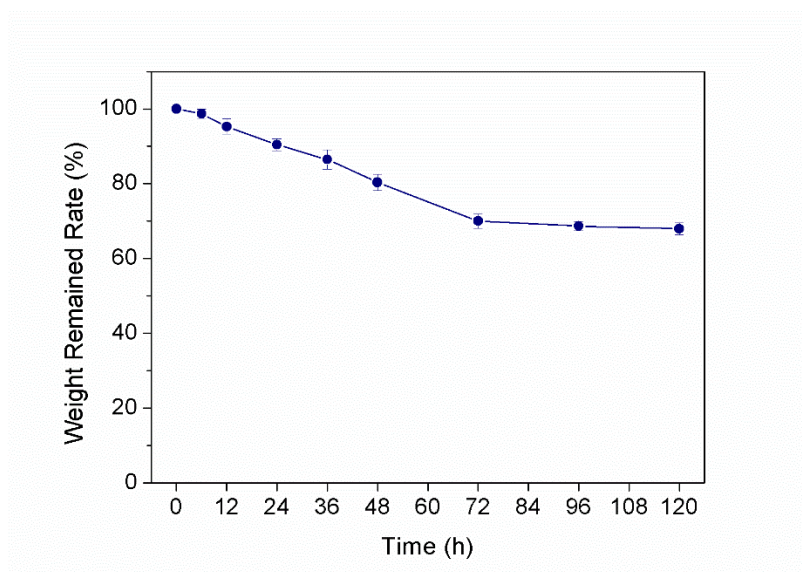


Figure S8, related to Figure 3. The weight remained rate profile of hybrid hydrogel in PBS was used to evaluate its degradation behavior.

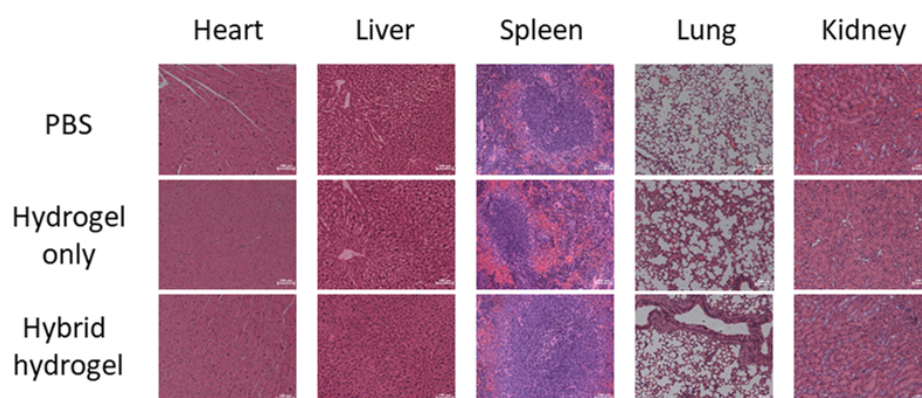


Figure S9, related to Figure 3. Representative H&E-stained images of different organs at day 12. Scale bar 100 μ m.